A Posteriori Error Estimation via Nonlinear Error Transport with Application to Shallow Water

J. W. Banks, J. A. F. Hittinger, J. M. Connors, and C. S. Woodward

Abstract. Numerical error estimation for time dependent hyperbolic problems is challenging for theoretical and practical reasons. In these systems, error can propagate long distances and produce effects far from the point of generation. In addition, nonlinear interactions of error, as well as discretization nonlinearities can play important roles and must be addressed. In this work, we investigate the use of error transport equations for *a posteriori* error estimation. We discuss the inclusion of nonlinearities in the error equations, which are particularly important for situations where local errors become large, such as near shocks.

1. Introduction

Error estimation for numerical approximations to partial differential equations is an important topic of research within the scientific computing community. Estimates of error can be useful in many ways, including adaptive gridding, model refinement, resource allocation decisions, and uncertainty quantification. For time dependent hyperbolic problems, errors can be generated locally and propagate long distances. For such systems, error transport has been developed as an effective way to incorporate the effect of error propagation [**15, 11, 8**]. In recent work [**5**], nonlinear error propagation was shown to be an important extension to the more traditional linear transport. Indeed, incorporating the effect of nonlinear error interactions was found to be critical to developing an accurate estimate of the error for some cases. In the current work, we extend the ideas of nonlinear error transport presented in [**5**] and include results for the shallow water equations in two space dimensions.

The remainder of this paper is organized as follows. In Section 2, we present the basic concepts of nonlinear error transport. Section 3 presents the shallow water equations in 2D. The error equations for the shallow water example are introduced in Section 4, and their discretization is described in Section 5. Section 6 shows

2010 *Mathematics Subject Classification.* Primary 65M12, 65M08; Secondary 76M12, 35L40.

Key words and phrases. a posteriori error estimation, hyperbolic equations, finite volume methods, finite difference methods, weak solutions.

This work was performed under the auspices of the U.S. Department of Energy by Lawrence Livermore National Laboratory under Contract DE-AC52-07NA27344 and was funded by the Uncertainty Quantification Strategic Initiative Laboratory Directed Research and Development Project at LLNL under project tracking code 10-SI-013.

numerical results, including a verification study and results for a problem whose solution transitions from smooth to discontinuous. Conclusions are presented in 7.

2. Nonlinear Error Transport

The basic idea of error transport is to formulate an auxiliary PDE describing the evolution of the error. Numerical approximations to the original PDEs and error equations are then advanced in tandem. Traditionally the error equations have been linearized [**15, 11, 8**], but more recent work [**5**] investigated the use of the full nonlinear error equations.

To introduce the method, consider an evolution equation for $u(x,t)$ of the form

$$\partial_t u + \mathcal{F}(u) = 0, \tag{2.1}$$

where $\mathcal{F}(u)$ is some differential operator on u with initial conditions $u(x,t=0) = g(x)$ for $x \in \mathbb{R}$. Assuming $\tilde{u}(x,t)$ is an approximation to the true solution, the error is defined to be

$$e(x,t) = u(x,t) - \tilde{u}(x,t). \tag{2.2}$$

The error equations are found by substituting (2.2) into (2.1) to yield

$$\partial_t e + \mathcal{F}(e+\tilde{u}) - \mathcal{F}(\tilde{u}) = -\left(\partial_t \tilde{u} + \mathcal{F}(\tilde{u})\right). \tag{2.3}$$

Here $\mathcal{F}(\tilde{u})$ has been subtracted from both sides to show that in the linear case the error and primal solutions evolve by the same differential operator.

In linear error transport, Equation (2.3) is expanded in a Taylor series for small e, and terms that are nonlinear in e are discarded. This approach is valid when e is small. However, for many cases of practical interest, such as when weak solutions containing discontinuities are sought, the local error in a vicinity of the jump may be as large as the solution itself. For these cases, the expansion breaks down, and the resulting linear error equations are not an accurate description of the true error. Nonlinear error transport [**5**] was developed to address these concerns and uses the full nonlinear error equations (2.3).

2.1. A simple example. In order to discuss the potential importance of error nonlinearity consider the inviscid 1-D Burgers' equation,

$$\partial_t u + \partial_x \left(\frac{1}{2}u^2\right) = 0, \qquad x \in \mathbb{R}, \quad t > 0. \tag{2.4}$$

The error equation is

$$\partial_t e + \partial_x \left(\frac{1}{2}e^2 + \tilde{u}e\right) = -\partial_t \tilde{u} - \partial_x \left(\frac{1}{2}\tilde{u}^2\right). \tag{2.5}$$

We approach discretization using a method-of-lines formulation and the standard 4-stage RK-4 time integrator [**1**]. Note that single step schemes are also possible using a space-time, or modified equation, time-stepper (refer to [**5**] for details). Let $u_i \approx u(x_i,t)$ and $e_i \approx e(x_i,t) = u(x_i,t) - u_i$. Furthermore, let D_0, D_+, and D_- represent the usual centered, forward, and backward difference operators defined

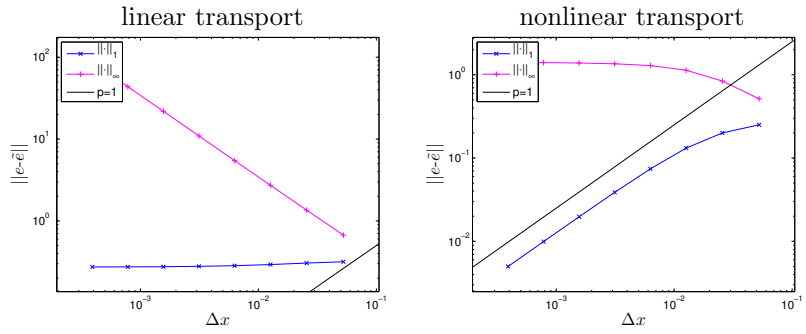

FIGURE 1. Convergence of the approximate error using linear error transport (left), and approximate error using nonlinear error transport (right). Results are presented at $t = 0.5$ for Burgers' equation with initial data $u(x, t = 0) = -\sin(\pi x)$.

by

$$2\Delta x D_0(u_i) = (u_{i+1} - u_{i-1}),$$
$$\Delta x D_+(u_i) = (u_{i+1} - u_i),$$
$$\Delta x D_-(u_i) = (u_i - u_{i-1}).$$

Discretization of (2.4) and (2.5) can be accomplished using the conservative formulation

$$\partial_t u_i = -D_+ \left(\frac{1}{2}(u_{i-1/2})^2 \right), \tag{2.6}$$

and

$$\partial_t e_i = -D_+ \left(\frac{1}{2}(e_{i-1/2})^2 + \hat{u}_{i-1/2} e_{i-1/2} \right) - \mathcal{R}_i, \tag{2.7}$$

where

$$\mathcal{R}_i = D_+ \left(\frac{1}{2}(u_{i-1/2})^2 \right) - D_0 \left(1 - \frac{\Delta x^2}{6} D_+ D_- \right) \left(\frac{1}{2}(u_i)^2 \right).$$

The quantities $u_{i-1/2}$ and $e_{i-1/2}$ are given by the solution to local Riemann problems at cell faces, and $\hat{u}_{i-1/2} = \frac{1}{2}(u_{i-1} + u_i)$ is a second-order accurate approximation to u at the cell face.

We perform a convergence test for the problem $u(x, t = 0) = -\sin(x)$ using both linear and nonlinear transport. Note that linear transport can be achieved by simply omitting terms in (2.5) that are nonlinear in e. Figure 1 shows these results at $t = 0.5$ after the formation of a shock in the exact solution. This figure shows the importance of error nonlinearity in that nonlinear transport converges as expected, while linear transport fails to converge in the L_1 norm and diverges in the max-norm.

3. Shallow Water Equations

An interesting example of nonlinear systems in two space dimension are the shallow water equations. This system sits at the core of climate codes, and estimating the error in simulation results can be important in climate studies. The

basic equations can be written as

$$\partial_t \mathbf{u} + \partial_x \mathbf{f}(\mathbf{u}) + \partial_y \mathbf{g}(\mathbf{u}) = 0, \tag{3.1}$$

where

$$\mathbf{u} =, \begin{bmatrix} \eta \\ \eta u \\ \eta v \end{bmatrix}, \quad \mathbf{f}(\mathbf{u}) = \begin{bmatrix} \eta u \\ \frac{1}{2} g\eta^2 + \eta u^2 \\ \eta uv \end{bmatrix}, \quad \mathbf{g}(\mathbf{u}) = \begin{bmatrix} \eta v \\ \eta uv \\ \frac{1}{2} g\eta^2 + \eta v^2 \end{bmatrix}.$$

Here η represents the height of the water surface above a given bathymetry (flat in this case), (u, v) represents the velocity, and g is a given constant acceleration due to gravity. The eigenstructure of the flux Jacobian is given by

$$\frac{\partial \mathbf{f}}{\partial \mathbf{u}} = \begin{bmatrix} 1 & 0 & 1 \\ u-c & 0 & u+c \\ v & 1 & v \end{bmatrix} \begin{bmatrix} u-c & 0 & 0 \\ 0 & u & 0 \\ 0 & 0 & u+c \end{bmatrix} \begin{bmatrix} \frac{u+c}{2c} & -\frac{1}{2c} & 0 \\ -v & 0 & 1 \\ -\frac{u-c}{2c} & \frac{1}{2c} & 0 \end{bmatrix},$$

where $c = \sqrt{g\eta}$. A similar result is found for the y-direction. Therefore the equations are hyperbolic when $g\eta > 0$. In addition, the system is seen to support a linear wave traveling at the local velocity and nonlinear "acoustic" waves traveling at the local velocity plus/minus c. More details on the equations and characteristic analysis can be found in [**14**], for example.

4. Error Equations for Shallow Water

In order to derive the error equations for the shallow water equations, we make the familiar *ansatz* that $\mathbf{u} = \tilde{\mathbf{u}} + \mathbf{e}$. Here $\mathbf{e}$ is a vector of errors in the conserved variables. Substitution into (3.1) yields the error equation

$$\partial_t \mathbf{e} + \partial_x \mathbf{F}(\mathbf{e}, \tilde{\mathbf{u}}) + \partial_y \mathbf{G}(\mathbf{e}, \tilde{\mathbf{u}}) = -\partial_t \tilde{\mathbf{u}} - \partial_x \mathbf{f}(\tilde{\mathbf{u}}) - \partial_y \mathbf{g}(\tilde{\mathbf{u}}) \tag{4.1}$$

$$\begin{aligned} \mathbf{F}(\mathbf{e}, \tilde{\mathbf{u}}) &= \mathbf{f}(\mathbf{e} + \tilde{\mathbf{u}}) - \mathbf{f}(\tilde{\mathbf{u}}), \\ \mathbf{G}(\mathbf{e}, \tilde{\mathbf{u}}) &= \mathbf{g}(\mathbf{e} + \tilde{\mathbf{u}}) - \mathbf{g}(\tilde{\mathbf{u}}). \end{aligned} \tag{4.2}$$

Equation (4.1) is a forced nonlinear evolution equation describing the evolution of the error in relation to the given approximation $\tilde{\mathbf{u}}$.

5. Discretization

Discretization of the governing and error equations is accomplished using conservative finite differences in space, and the standard four-stage RK-4 time integration. Succinctly the semi-discrete form is

$$\partial_t \mathbf{u}_{i,j} = -D_{+x} \mathbf{f}(\mathbf{u}_{i-1/2,j}) - D_{+y} \mathbf{g}(\mathbf{u}_{i,j-1/2}), \tag{5.1}$$

$$\partial_t \mathbf{e}_{i,j} = -D_{+x} \mathbf{F}(\mathbf{e}_{i-1/2,j}, \hat{\mathbf{u}}_{i-1/2,j}) - D_{+y} \mathbf{G}(\mathbf{e}_{i,j-1/2}, \hat{\mathbf{u}}_{i,j-1/2}) - \mathcal{T}_{i,j}, \tag{5.2}$$

where D_{+x} and D_{+y} are the divided differences in the x- and y-coordinate directions, respectively, $\hat{\mathbf{u}}_{i-1/2,j} = \frac{1}{2}(\mathbf{u}_{i-1,j} + \mathbf{u}_{i,j})$, $\hat{\mathbf{u}}_{i,j-1/2} = \frac{1}{2}(\mathbf{u}_{i,j-1} + \mathbf{u}_{i,j})$, and $\mathcal{T}_{i,j}$ is an approximation to the residual derived in a similar manner as in Section 2:

$$\begin{aligned} \mathcal{T}_{i,j} =& D_{+x} \mathbf{f}(\mathbf{u}_{i-1/2,j}) - D_{0x} \left(1 - \frac{\Delta x^2}{6} D_{+x} D_{-x}\right) \mathbf{f}(\mathbf{u}_{i,j}) + \\ & D_{+y} \mathbf{g}(\mathbf{u}_{i,j-1/2}) - D_{0y} \left(1 - \frac{\Delta y^2}{6} D_{+y} D_{-y}\right) \mathbf{g}(\mathbf{u}_{i,j}). \end{aligned} \tag{5.3}$$

The values at the half points are determined through the solution of local Riemann problems. For example, consider $\mathbf{u}_{i-1/2,j}$ and $\mathbf{e}_{i-1/2,j}$ (all others are similarly derived). The left and right states for the primal Riemann problem are denoted $\mathbf{u}_L = \mathbf{u}_{i-1+,j}$ and $\mathbf{u}_R = \mathbf{u}_{i-,j}$, respectively, while for the error equation they are $\mathbf{e}_L = \mathbf{e}_{i-1+,j}$ and $\mathbf{e}_R = \mathbf{e}_{i-,j}$, respectively. These states are defined using

$$\mathbf{u}_{i\pm,j} = \mathbf{u}_{i,j} \pm \frac{1}{2} R_{i,j}\Lambda_{i,j}\psi\left(R_{i,j}^{-1}\Delta x D_+ u_{i,j}, R_{i,j}^{-1}\Delta x D_- u_{i,j}\right), \tag{5.4}$$

$$\mathbf{e}_{i\pm,j} = \mathbf{e}_{i,j} \pm \frac{1}{2} R_{i,j}\Lambda_{i,j}\psi\left(R_{i,j}^{-1}\Delta x D_+ e_{i,j}, R_{i,j}^{-1}\Delta x D_- e_{i,j}\right), \tag{5.5}$$

where the function ψ can be used to vary the algorithm between first-order, second-order, and a nonlinear TVD method through the choice of ψ:

$$\begin{aligned}\psi_1(a,b) &= 0,\\ \psi_2(a,b) &= \frac{1}{2}(a,b),\\ \psi_{MM}(a,b) &= \text{minmod}\,(a,b).\end{aligned}$$

See [**2**] for additional details of this approach. Note that $R_{i,j}\Lambda_{i,j}R_{i,j}^{-1} = \frac{\partial \mathbf{f}}{\partial \mathbf{u}}(\mathbf{u}_{i,j})$ depend only on $\mathbf{u}_{i,j}$ and not on the error. This choice has no affect on the formal accuracy of the method, and is made because the eigenvalues are real only when η is positive. In practice it is often the case that the discrete solution $\mathbf{u}$ adheres to these bounds, but this may not be the case for $\mathbf{u}+\mathbf{e}$.

Our approximate solutions to local Riemann problems make use of a Roe averaged linearization [**12, 13**]. The Roe averaged state, $\mathbf{u}_*$, is given by

$$\begin{aligned}\eta_* &= \frac{1}{2}\left(u_L + u_R\right),\\ u_* &= \frac{\sqrt{\eta_L}u_L + \sqrt{\eta_R}u_R}{\sqrt{\eta_L}+\sqrt{\eta_R}},\\ v_* &= \frac{\sqrt{\eta_L}v_L + \sqrt{\eta_R}v_R}{\sqrt{\eta_L}+\sqrt{\eta_R}}.\end{aligned}$$

Define characteristic quantities $\mathbf{w}_L = R_*^{-1}\mathbf{u}_L$, $\mathbf{w}_R = R_*^{-1}\mathbf{u}_R$, $\mathbf{q}_L = R_*^{-1}\mathbf{e}_L$, and $\mathbf{q}_R = R_*^{-1}\mathbf{e}_R$ where $R_*\Lambda_*R_*^{-1} = \frac{\partial \mathbf{f}}{\partial \mathbf{u}}(\mathbf{u}_*)$. The solution to the primal Riemann problem is given by

$$\hat{\mathbf{w}}^{(k)} = \begin{cases} \mathbf{w}_L^{(k)} & \text{if} \quad \Lambda_*^{(k,k)} > 0,\\ \mathbf{w}_R^{(k)} & \text{if} \quad \Lambda_*^{(k,k)} \le 0,\end{cases} \tag{5.6}$$

where the superscripts k are used to denote component number. The solution to the error Riemann problem is given by

$$\hat{\mathbf{q}}^{(k)} = \begin{cases} \mathbf{q}_L^{(k)} & \text{if} \quad \Lambda_*^{(k,k)} > 0,\\ \mathbf{q}_R^{(k)} & \text{if} \quad \Lambda_*^{(k,k)} \le 0.\end{cases} \tag{5.7}$$

The final update is then completely prescribed by assigning $\mathbf{u}_{i-1/2,j} = R_*\hat{\mathbf{w}}$ and $\mathbf{e}_{i-1/2,j} = R_*\hat{\mathbf{q}}$.

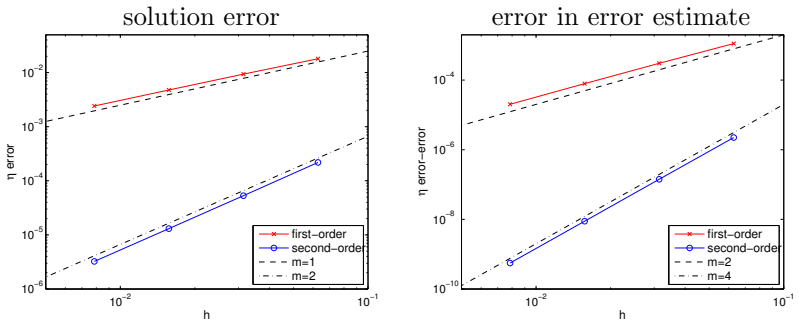

FIGURE 2. Verification using MMS. Results are shown using the first-order, and second-order schemes. The error in the primal approximation converges at the expected rate, and the error in the error estimate doubles that.

6. Results

To demonstrate the validity of our approach to error estimation, we now present results from a number of numerical experiments. We begin with a verification study using the method of manufactured solutions (MMS) and then proceed to a somewhat more physically relevant test case that evolves from smooth to discontinuous as a result of nonlinearities in the operator.

6.1. Verification. In order to verify the overall implementation, we use the MMS, sometimes called twlilight zone [**7, 9**], whereby a known smooth solution is assumed as the exact answer. The source term necessary to yield this solution is easily derived and added the the governing equations. We make the following choice

$$\eta = 1 + \frac{1}{10}\cos(x)\sin\left(y - \frac{1}{2}\right)\sin(t),$$
$$u = 2\cos\left(x - \frac{1}{2}\right)\sin(y)\sin(2t),$$
$$v = \cos\left(x - \frac{1}{4}\right)\sin\left(y - \frac{1}{4}\right)\sin(3t),$$

where the offset in η is chosen to bound η away from zero so that the governing equations remain well-posed. The periodic simulation domain is chosen to be $(x, y) \in (-\pi, \pi) \times (-\pi, \pi)$, and the exact solution is imposed as an initial condition. As is typical in the literature, limiting is not used for MMS verification tests because nonlinearities in the method produce locally reduced rates that can be difficult to interpret [**6, 4**]. Convergence results using the first- and second-order schemes and the L_∞ norm are presented in Figure 2. The primal approximations from the first- and second- order schemes are seen to converge at $O(h)$ and $O(h^2)$ respectively, while the error estimates are seen to converge at $O(h^2)$ and $O(h^4)$ respectively. This is the expected behavior as shown in [**5**] using Taylor series analysis.

6.2. Gaussian hump. Consider now the unforced shallow water equations with zero initial velocity and a Gaussian hump for vertical displacement,

$$\eta(x, y, 0) = \frac{1}{10}\left(\exp\left(-\frac{25}{8}\left(x^2 + y^2\right)\right) + \frac{1}{10}\right).$$

Due to nonlinearities in the governing equations, the solution to this problem develops a discontinuity at finite time. We do not know the exact solution to this problem and instead choose to use Richardson extrapolation to indicate the efficacy of our error estimation procedure. As described in [**4, 10**], Richardson extrapolation can be used to estimate the error in a numerical approximation given three resolutions. This estimated error can then be compared against the error estimate produced using evolution.

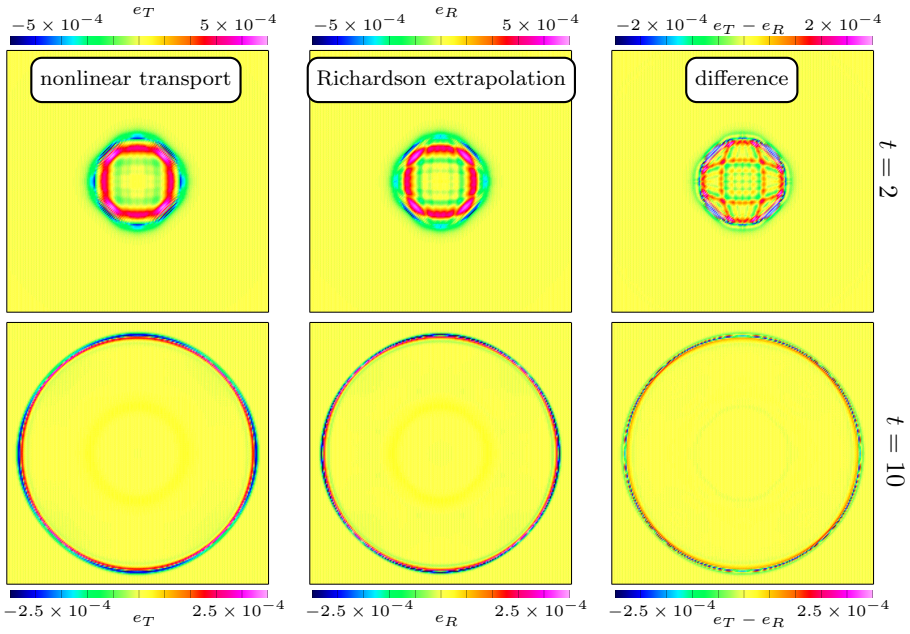

FIGURE 3. Comparison of error estimates for η before shock formation at $t = 2$ (top), and after shock formation at $t = 10$ (bottom). Shown are results for nonlinear error transport (left), Richardson extrapolation (center), and their difference (right).

Figure 3 shows such a comparison on a domain $(x, y) \in (-\pi, \pi) \times (-\pi, \pi)$. Results from nonlinear error transport are shown using 200 points in each direction, and this is also the base resolution for the Richardson estimate. The subsequent two resolutions for Richardson use 400 and 800 points, respectively. We show only results for the nonlinear high-resolution scheme. For many applications, such a scheme is the most practical. In addition, the inherent nonsmooth nature of the errors in such a scheme leads to interesting results for error estimators. For early times ($t = 2$), the solution to this test problem is smooth, and Figure 3 shows good agreement between the two techniques despite the difficulties imposed by discontinuous limiting. At later times ($t = 10$), the solution develops a discontinuity.

Despite the discontinuous nature of the solution, the nonlinear error transport approach is shown to estimate the magnitude and location of the error near the shock. Note that in applying Richardson extrapolation for discontinuous solutions great care must be exercised, and we follow the prescription in [**3**].

7. Conclusions

We have discussed the use of nonlinear error transport as an error estimation technique. The need to include nonlinear error interactions was motivated by the Burgers' equation in 1D. Extension to the 2D shallow water equations was then discussed. The approach was verified using MMS for a smooth problem. In addition, we presented results for a more challenging test problem with no known solution. Here the exact solution transitioned from smooth to discontinuous, and the scheme was shown to still provide reasonable error estimates.

References

1. U. M. Ascher and L. R. Petzold, *Computer methods for ordinary differential equations and differential-algebraic equations*, SIAM, Philadelphia, 1998.
2. B. van Leer, *Towards the ultimate conservative difference scheme, V. A second-order sequel to Godunov's method*, J. Comput. Phys. **32** (1979), 101–136.
3. J. W. Banks and T. D. Aslam, *Richardson extrapolation for linearly degenerate discontinuities*, SIAM J. Sci. Comput. (submitted), arXiv:1205.6504v1.
4. J. W. Banks, W. D. Henshaw, and J. N. Shadid, *An evaluation of the FCT method for high-speed flows on structured overlapping grids*, J. Comput. Phys. **228** (2009), no. 15, 5349–5369.
5. J. W. Banks, J. A. F. Hittinger, J. M. Connors, and C. S. Woodward, *Numerical error estimation for nonlinear hyperbolic PDEs via nonlinear error transport*, Comput. Method. Appl. Mech. Engrg. **213–216** (2012), 1–15.
6. J. W. Banks, D. W. Schwendeman, A. K. Kapila, and W. D. Henshaw, *A high-resolution Godunov method for compressible multi-material flow on overlapping grids*, J. Comput. Phys. **223** (2007), 262–297.
7. G. Chesshire and W. Henshaw, *Composite overlapping meshes for the solution of partial differential equations*, J. Comput. Phys. **90** (1990), 1–64.
8. A. Hay and M. Visonneau, *Error estimation using the error transport equation for finite-volume methods and arbitrary meshes*, Int. J. Comput. Fluid D. **20** (2006), no. 7, 463–479.
9. W. D. Henshaw, *A fourth-order accurate method for incompressible navier-stokes equations on overlapping grids*, J. Comput. Phys. **113** (1994), 13–25.
10. William D. Henshaw and Donald W. Schwendeman, *Parallel computation of three-dimensional flows using overlapping grids with adaptive mesh refinement*, J. Comput. Phys. **227** (2008), no. 16, 7469–7502.
11. Y. Qin and T. I-P. Shih, *A method for estimating grid-induced errors in finite-difference and finite-volume methods*, AIAA Paper 2003-0845, 2003.
12. P. L. Roe, *Approximate Riemann solvers, parameter vectors, and difference schemes*, J. Comput. Phys. **43** (1981), 357–372.
13. E. F. Toro, *Riemann solvers and numerical methods for fluid dynamics*, Springer, Berlin, 1999.
14. G. B. Whitham, *Linear and nonlinear waves*, Wiley-Interscience, New York, 1974.
15. X. D. Zhang, J.-Y. Trépanier, and R. Camarero, *A posteriori error estimation for finite-volume solutions of hyperbolic conservation laws*, Comput. Method. Appl. Mech. Engrg. **185** (2000), 1–19.

Center for Applied Scientific Computing, Lawrence Livermore National Laboratory, Livermore, CA 94551

E-mail address: banks20@llnl.gov